Kinetics and Thermodynamics of Adsorption of Fuchsin Acid on Nickel Oxide Nanoparticles

Babak Samiey and Saeid Farhadi

Department of Chemistry, Faculty of Science, Lorestan University, 68137-17133, Khoramabad, Iran

* Corresponding author: E-mail: babsamiey@yahoo.com

Abstract

NiO nanoparticle was used to adsorb fuchsin acid (FA) from aqueous solution. In the used concentration range of FA, its adsorption isotherms on NiO nanoparticles were three-region. NiO nanoparticle was prepared via the thermal decomposition of the tris(ethylenediamine)Ni(II) nitrate complex as a new precursor. In this work, effects of temperature, concentration, particle size, shaking rate, contact time, pH of the solution were investigated. Adsorption process was exothermic in the first and second regions and endothermic in the third region. Adsorption kinetics was studied by a number of equations including the KASRA, pseudo-first-order, pseudo-second-order, Elovich, Avrami and pore-diffusion equations. Adsorption acceleration and adsorption velocity values of this process were obtained by the KASRA equation and it was shown that with increase in FA concentration or temperature or shaking rate, initial adsorption velocity values of process increase.

Keywords: Adsorption; Fuchsin acid; NiO nanoparticle; KASRA model

1. Introduction

Large amount of colored effluent originated from different dye manufacturing units are charged into in the ecosystem and because of their toxicity and mutagenicity[1,2] cause environmental danger. Dyes are used in different industries such as paper, plastics, leather, pharmaceutical, food, cosmetics, dyestuffs, textiles, etc. In general, the dyes chosen by industries have good stability and fastness. Once it enters water body as a pollutant, the destruction of these dyes poses a problem. Various chemical, physical and biological treatment methods have developed for the removal of dyes from aqueous solutions, including adsorption,[3] membrane filtration,[4] oxidation with ozone,[5] ozonation,[6] photocatalytic degradation,[7] and reverse osmosis[8] and biodegradation.[9] The degradation by-products of organic dyes such as synthetic azo-dyes have dangerous impacts on the environment. Fuchsin acid (FA), an acid dye, is used as a copper corrosion inhibitor,[10] biological stains, sometimes as a and for dyeing textiles[11] and formation of organic–inorganic hybrid nanocomposite.[12] Chemical structure of FA is shown in Figure 1.

Adsorption, due to its low cost, simplicity of design and ease of operation is a reliable treatment technique.
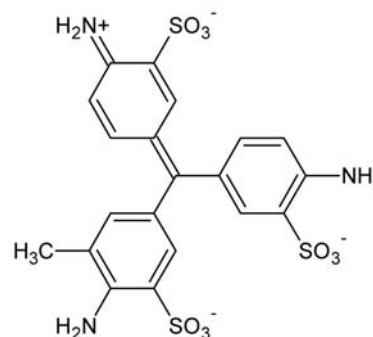

Figure 1: Molecular structure of fuchsin acid.

Nanoparticle research is an area of intense scientific interest due to a wide variety of potential applications in different fields of science. The interesting and sometimes unexpected properties of nanoparticles are largely due to the large surface area of the material, which dominates the contributions made by the small bulk of the material. In recent years, there has been emphasis on the application of nanoparticles as efficient adsorbents. A number of these materials such as NiO,[13] gold,[14] chitosan,[15] multiwall carbon nanotube/iron oxide magnetic composite,[16] maghemite,[17] MgO,[18] TiO_2,[19] clay,[20] Multi-walled carbon na-

notubes,[21] hydroxyapatite,[22] manganese dioxide,[23] alumina[24] and magnesium silicate[25] nanoparticles have been tested for the adsorption of other compounds. It has been proven that they are effective adsorbents for the removal of dyes and metallic pollutants from aqueous solutions. In this study, we used nickel oxide nanoparticle as adsorbent. Nickel oxide (NiO) is one of the most important transition metal oxides due to its applications in diverse fields, including catalysis,[26] fuel cell electrodes,[27] gas sensors,[28] battery cathodes,[29] magnetic materials[30] and smart windows.[31] NiO nanoparticles show a ferromagnetic behavior and could be a promising photocatalytic material.[32]

The aim of this work is to estimate adsorption capacity of NiO nanoparticles for FA. These particles showed the highest adsorption capacities of FA compared to many other adsorbents. In order to investigate the mechanism of adsorption process, in addition to conventional kinetic and thermodynamic equations, a new kinetic model was introduced. Furthermore, an optimization of the process was attempted through tuning a series of parameters such as size of NiO nanoparticles, dye concentration, temperature and initial pH values.

2. Materials and Methods

2. 1. Materials

Ni(NO$_3$)$_2$.6H$_2$O, ethylenediamine, ethanol (99.9%), ether, HCl and fuchsin acid were purchased from Merck. All chemicals were used without further purification.

2. 2. Preparation of NiO nanoparticles

An aqueous solution of Ni(NO$_3$)$_2$.6H$_2$O is treated with a slight stoichiometric excess of ethylenediamine (en) and the resultant deep-purple [Ni(en)$_3$](NO$_3$)$_2$ was precipitated by slow addition of ethanol. After standing for several hours in the cold, the crystals were filtered on a Buchner funnel, washed with ethanol, ether and dried in the open air at 50 °C. The complex was decomposed at 250, 400 and 600 °C. In the XRD spectra of the sample prepared in 250 °C, peaks attributable to metallic nickel are observed, Figure 2. The above protocol was described by Farhadi et al.[32]

2. 3. Characterization of NiO Nanoparticles

X-ray powder diffraction (XRD) patterns were recorded using a Rigaku D-max C III, X-ray diffractometer using Ni-filtered Cu K α radiation (λ = 1.5406 Å) to determine the phases present in the decomposed samples. The average sizes of NiO particles were estimated to be about 25.1, 13.1 and 30.3 nm at 250, 400 and 600 °C respectively, by Debye–Scherrer formula:[33]

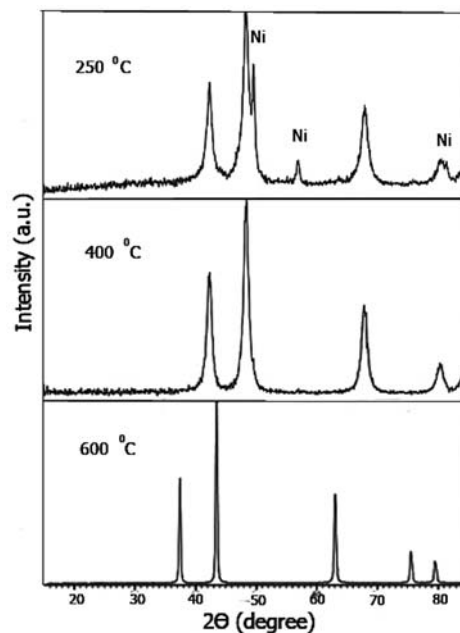$$D_{XRD} = \frac{0.9\lambda}{\beta \cos\theta} \qquad (1)$$

Figure 2: XRD patterns for [Ni(en)$_3$](NO$_3$)$_2$ decomposed at selected temperatures.

where D_{XRD} is the average crystalline size, λ is the wavelength of Cu K α, β is the full width at half maximum (FWHM) of the diffraction peak and θ is the Bragg's angle. Increasing the calcination temperature up to 600 °C causes conglomeration of NiO nanoparticles which increases their size.[34] Infrared spectra were recorded on a Shimadzu system FTIR-8400S spectrophotometer using KBr pellets.

2. 4. Adsorption Experiments

In adsorption experiments, 10 ml of FA solution of different initial concentrations was transferred to a series of 15-ml glass stoppered bottles, each containing 0.0025 g of NiO sample. The solutions were shaken at 80 rpm in a temperature controlled shaking water bath (Fater electronic Co., Persian Gulf model) at 308, 318 and 328 K within ±0.1 K for 20 h to reach equilibrium under experimental conditions. The initial concentrations of FA were in the concentration range of 1.9×10^{-6} –9.3×10^{-5} M. After adsorption, the concentration of FA in the residual solutions was determined by photometry (UV-Vis 160, Shimadzu) at its λ_{max} value in these solutions (544 nm). The adsorption capacity of FA on the adsorbent, q_e (mg g^{-1}), was calculated by a mass balance relation as follows

$$q_e = \frac{(c_0 - c_e)MV}{1000w} \qquad (2)$$

where c_0 and c_e are the initial and equilibrium concentrations of adsorbate (M) respectively, V is the volume of so-

lution (ml), *w* is the weight of the used adsorbent (g) and *M* is the molecular weight of adsorbate (mg mol^{-1}). In adsorption kinetic experiments, 10 ml of FA aqueous solution in the concentration range of 2.3×10^{-5} –4.6×10^{-4} M was transferred to a series of glass stoppered bottles, each containing 0.0025 g of NiO nanoparticle sample and solutions were shaken at 40, 80 and 120 rpm and different temperatures. At predetermined times, the contents of FA in the solutions were determined by photometry at its λ_{max} value. In these series of experiments, q_e and c_e in relation (2) are replaced by q_t (adsorption capacity at time *t*) and c_t (concentration of adsorbate at time *t*), respectively.

In this work, the results are studied by "*adsorption isotherm regional analysis model*" or abbreviated as ARIAN model.[35] This model is introduced for studying adsorption isotherms up to four regions. In ARIAN model which is explained briefly, it is assumed that region 1 obeys Henry's law:

$$q_e = Kc_e \tag{3}$$

where *K* is the binding constant of adsorbate on the surface and adsorption increases linearly with concentration. Region 2 starts from the *starting second region concentration* (abbreviated as *ssc*) point and when adsorbate is a surfactant, is specially named the *hemimicelle concentration* (abbreviated as *hmc*) point. This region includes only monolayer surface aggregate formation and can be studied by an appropriate isotherm such as the Langmuir, Temkin, Dubini-Radushkevich equations, etc. The Langmuir equation[36] in linearized form is given as

$$\frac{c_e}{q_e} = \frac{1}{q_{max}K} + \frac{c_e}{q_{max}} \tag{4}$$

where *K* is the Langmuir adsorption constant and q_{max} is the monolayer capacity. The Temkin equation[36] is represented by

$$q_e = c_1 \ln(c_2 c_e) \tag{5}$$

where c_1 is a constant and c_2 is adsorption equilibrium constant.

The Dubinin-Radushkevich equation[38,39] is used to estimate the characteristic porosity of the adsorbent and the apparent energy of adsorption. In this work, this equation is used for all regions. The equation is given by

$$q_D - B_D \left(RT \ln \left(1 + \frac{1}{c_e} \right) \right)^2 \tag{6}$$

where B_D is related to the free energy of adsorption per mole of adsorbate (mol^2 J^{-2}) and q_D is the theoretical monolayer saturation capacity. The apparent energy of adsorption from Dubinin-Radushkevich isotherm, *E*, (J mol^{-1}) can be computed using the relationship

$$E = \frac{1}{(2B_D)^{\frac{1}{2}}} \tag{7}$$

In region 3, new surface aggregates or admicelles and new surface clusters (in the case of surfactants) form. The *starting third region concentration* (abbreviated as *stc*) point defines beginning this region. These data are analyzed by the bilayer isotherm equation (Eq. 8) and those derived from it (Eqs. 9 and 10).[35] In the third region, assuming adsorption occurs mostly in the first and second layer, we have

$$\frac{c_e}{q_e} = \frac{1 + c_e K_{sa} + xc_e^2 K_{sa}}{q_{mon}K_{sa} + 2q_{mon}xc_e K_{sa}} \tag{8}$$

where q_{mon} and q_e are the monolayer and equilibrium adsorption capacity, respectively. K_{sa} and *x* are the adsorption equilibrium constants of adsorbate molecules in surface aggregates and in all layers above first one, respectively. If adsorbate molecules are adsorbed mostly on the first layer, equation (8) can be written as

$$\frac{c_e}{q_e} = \frac{1}{q_{mon}K_{sa}} + \frac{c_e}{q_{mon}} + \frac{xc_e^2}{q_{mon}} \tag{9}$$

which is used for low bilayer coverage (abbreviated as LBC) and if the adsorption process is monolayer, equation (8) can be reduced to

$$\frac{c_e}{q_e} = \frac{1}{q_{mon}K_{sa}} + \frac{c_e}{q_{mon}} \tag{10}$$

where equation (10) is a Langmuir-type equation and region 4 starts from maximum adsorption capacity and is as plateau or curve goes down.

3. Results and Discussion

3. 1. Adsorption Isotherm Modeling

Analysis of isotherm data is important for measuring the adsorption capacity of the adsorbent, which is one of the main parameters required for the design of an adsorption system. We used NiO nanoparticles formed at 400 °C as adsorbent because of its small size compared those formed at 250 and 600 °C. The q_e uptakes of FA by NiO nanoparticle (formed at 400 °C) in the initial FA concentration range of 2.3×10^{-5} –4.6×10^{-4} M in neutral aqueous solutions at 308, 318 and 328 K are illustrated in Figure 3.

Data were analyzed by ARIAN model and it was shown that adsorption isotherms of FA by NiO nanoparticle are three-region in the used concentration range of FA. By analysis of data of the first region by Henry's law the binding constant values of adsorption process in this region were obtained, Table 1, and using them ΔH and ΔS values are -10.2 kJ mol^{-1} and 108.2 J mol^{-1} K^{-1}, respectively.

Table 1. The *ssc* and q_{ssc} values and parameters obtained from the Henry's law and Dubinin-Radushkevich equation for adsorption of FA on NiO nanoparticles (formed at 400 °C) in the first region at 308–328 K.

T (K)	ssc (M)	q_{ssc} (mg g^{-1})	Henry's law			Dubinin-Radushkevich		
			K	A	R^2	$\ln q_D$	E	R^2
308	8.41×10^{-6}	195.3	2.48×10^7	-4.8	0.993	12.3	8.1	0.999
318	1.74×10^{-5}	281.7	2.14×10^7	5.7	0.990	9.6	10.5	0.999
328	1.64×10^{-5}	284.1	1.94×10^7	6.8	0.987	10.9	10.2	0.990

Dimensions of q_D and A are in mg g^{-1} and those of K and E are in mg g^{-1} M^{-1} and kJ mol^{-1}, respectively. Henry's law for experimental data is as $q_e = Kc_e + A$. Initial FA concentrations corresponding to *ssc* are 9.2×10^{-5}, 1.4×10^{-4} and 1.4×10^{-4} M at 308, 318 and 328 K, respectively.
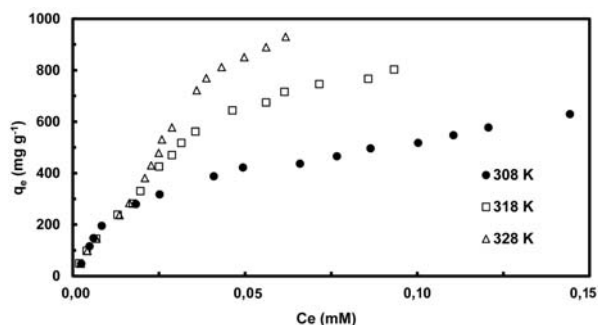
Figure 3: q_e versus c_e for adsorption of FA on NiO nanoparticles (formed at 400 °C) at different temperatures.

Data of the second region were fitted in the Temkin equation and binding constant values and the related thermodynamic parameters were obtained by this equation, Table 2.

ΔH and ΔS values of process in this region are -183.0 kJ mol^{-1} and –482.2 J mol^{-1} K^{-1}, respectively. Adsorption of too much FA molecules on the surface of NiO results in formation of new FA surface aggregates on its surface. This results in the formation of the third region.

The third region starts in q_e values 465.5, 561.7 and 812.7 mg g^{-1} and at 308, 318 and 328 K, respectively. In the third region, binding constant values were calculated by the Langmuir-like equation, Table 3, and ΔH and ΔS values of process in this region are 46.1 kJ mol^{-1} and 228.5 J mol^{-1} K^{-1}, respectively.

As reported before,[32] the specific surface area of the NiO nanoparticles is 84.5 m^2 g^{-1} and this results in their high q_{mon} values obtained from the Langmuir-type equation which are 1006.1–1379.3 mg g^{-1} at different temperatures, Table 3.

Adsorption capacity of NiO nanoparticle for FA is very high and in the FA used concentration range we could not obtain maximum experimental adsorption capacity of NiO nanoparticle for FA molecules and thus we did not observe the fourth region for these experiments. Thus, for comparative purposes, we used q_{mon} values calculated from Langmuir-like in the third region. The $\dfrac{q_{ssc}}{q_{mon}}$ values, which are proportional to the relative magnitude of the first region, are about 0.14 at 308, 318 and 328 K, Tables

Table 2. Parameters obtained from the Temkin, Langmuir and Dubinin-Radushkevich isotherms for adsorption of FA on NiO nanoparticles (formed at 400 °C) in the second region at 308–328 K.

T (K)	Temkin			Langmuir			Dubinin-Radushkevich		
	c_1	c_1	R^2	K	q_{max}	R^2	$\ln q_D$	E	R^2
308	123.9	547035	0.993	67742	529.1	0.988	7.8	13.5	0.992
318	4552.9	118550	0.998	714	23474.2	0.992	11.1	8.8	0.992
328	6692.6	94467	0.988	6907	2272.7	0.989	12.4	8.2	0.992

Dimension of c_1, q_{max} and q_D is in mg g^{-1}. Dimensions of c_2, K and E are in M^{-1}, M^{-1} and kJ mol^{-1}, respectively.

Table 3. The *stc* and q_{stc} values and parameters obtained from the Langmuir-like and Dubinin-Radushkevich isotherms for adsorption of FA on NiO nanoparticles (formed at 400 °C) in the third region at 308–328 K.

T (K)	stc (M)	q_{stc} (mg g^{-1})	Langmuir-type			Dubinin-Radushkevich		
			K_{sa}	q_{mon}	R^2	$\ln q_D$	E	R^2
308	7.67×10^{-5}	465.5	11094	1006.1	0.983	8.5	11.5	0.989
318	3.56×10^{-5}	561.7	31414	1071.8	0.989	8.3	13.9	0.976
328	4.32×10^{-5}	812.7	32955	1379.3	0.989	8.9	14.0	0.993

Dimensions q_{mon} and q_D are in mg g^{-1}. Dimensions of K_{sa} and E are in M^{-1} and kJ mol^{-1}, respectively. Initial FA concentrations corresponding to *stc* are 2.8×10^{-4}, 2.8×10^{-4} and 3.9×10^{-4} M at 308, 318 and 328 K, respectively.

1 and 3. The $\dfrac{q_{stc} - q_{ssc}}{q_{mon}}$ values, which are proportional to the relative magnitude of the second region, are about 0.32, 0.39 and 0.45 at 308, 318 and 328 K, Tables 1, 2 and 3.

As given in Tables 1, 2 and 3, binding constant values of FA to the surface decrease from the first to the third region because the negatively charged surface increases progressively with adsorption of a large number of FA molecules. But, due to hydrophobic interactions between adsorbed FA molecules the process in this region is endothermic and the relative magnitude of this region is 0.54, 0.47 and 0.41 at 308, 318 and 328 K respectively.

NiO nanoparticle shows amphoteric behavior in aqueous media. The point of zero charge (pzc) of NiO nanoparticle, i.e. the point at which the surface charge is neutral, is 10.5[40] and for lower pH values, surface of NiO nanoparticle is in the protonated form ($NiOH_2^+$) This study was carried out in neutral aqueous solutions. As seen in Figure 4, peak of hydroxyl groups at 3558.42 cm^{-1} in FTIR spectrum of NiO shifts to 3504.42 cm^{-1} in FTIR spectrum of FA-adsorbed NiO.

This is due to electrostatic interaction of negatively charged FA molecules with $-OH$ and $-OH_2^+$ surface groups of NiO surface. This interaction has chemical nature and apparent energy of adsorption from Dubinin-Ra-
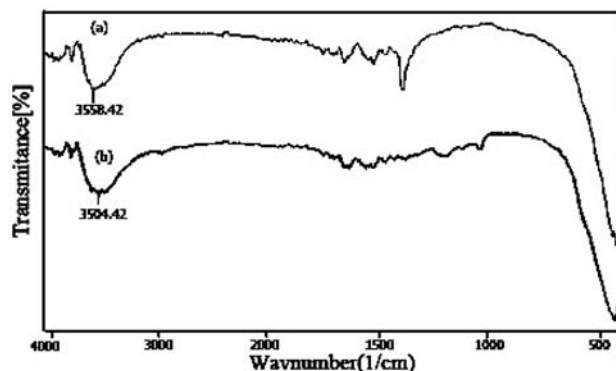

Figure 4: FTIR spectra of (a) [Ni(en)$_3$](NO$_3$)$_2$ decomposed at 400 °C and (b) its FA-adsorbed form.

dushkevich isotherm, is in the range of 8.2–14.0 kJ mol^{-1} at different temperatures and regions, Tables 1, 2 and 3. Our tests showed that NiO nanoparticle dissolves in acidic media and thus FA uptake (adsorbed on initially 0.0025 g NiO added as adsorbent in 10-ml samples) decreases, Figure 5, and the NiO used as adsorbent completely dissolves in 1M HCl.

3. 2. Adsorption Kinetic Equations

In this work, a new model and a new equation are introduced for study of adsorption kinetics. The proposed model is named "*Kinetics of Adsorption Study in the Regions with Constant Adsorption Acceleration*" or abbreviated as KASRA model. KASRA model is based on the following assumptions: (1) each time range that adsorption acceleration in it is constant, is named a *"region"*, (2) there are two regions before attaining plateau region[41] and (3) the boundaries between the first and second regions and the second and third (plateau) regions are named *starting second region* (abbreviated as *ssr*) and *kinetics of adsorption termination* (abbreviated as *kat*) points, respectively and are determined by the KASRA equation, Figure 6.

It is good to say that KASRA is a Persian word meaning king. To derive KASRA equation, a region with constant acceleration of adsorption is considered and we can write:

$$\frac{d^2 q_t}{dt^2} = a_i \qquad (11)$$

where a_i is acceleration of adsorption kinetics in the *ith* region and $i = 1–3$. Because of decrease in adsorbent concentration during adsorption process a_i values are negative in sign. In these cases, adsorption kinetics profile in the related region is concave downward. But, in some cases, the first region of adsorption kinetics diagram is concave upward or diagram in this region may be linear[42] and thus according to KASRA model, the related a_1 values are positive or zero, respectively. In such cases, for example
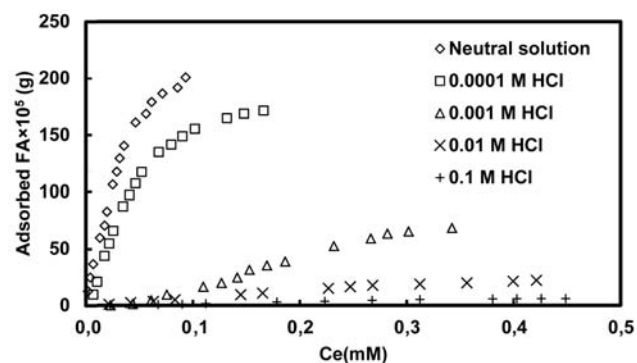

Figure 5: Adsorbed FA versus c_e for adsorption of FA on NiO nanoparticles (formed at 400 °C) at 318 K in different concentrations of HCl.
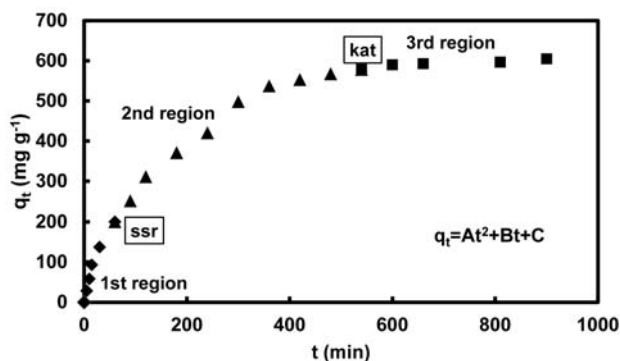
Figure 6: Schematic diagram of adsorption kinetics using KASRA model. Here, $a_1 < 0$ and ♦,▲ ■ symbols refer to the first, second and third regions, respectively.

multilayer adsorption of colloidal gold particles on silica,[42] or adsorption of some surfactants in concentrations above their cmc,[43] initial adsorption of adsorbate molecules facilitates adsorption of other ones and interaction between them acts as a driving force and increases the number of adsorbate molecules and thus a_1 for this case is written as

$$a_1 = a_{1s} + a_{1a} \tag{12}$$

where a_{1s} and a_{1a} are surface site and adsorbate-induced adsorption accelerations in the first region, respectively. If $|a_{1s}| < a_{1a}$ then $a_1 > 0$ and if $|a_{1s}| = a_{1a}$ then $a_1 = 0$. Similar situation is seen in the isothermal crystallization process in semicrystalline polymers[44–46] that is divided to primary and secondary nucleation processes and in the first times of these processes their plots are concave upward or linear. Finally, if $|a_{1s}| \gg a_{1a}$ then $a_1 \approx a_{1s} < 0$.

After integration and applying boundary condition $v_i = v_{0i}$ at $t = t_{0i}$, equation (11) becomes

$$v_i = \frac{dq_t}{dt} = a_i t + v_{0i} - a_i t_{0i} \tag{13}$$

where v_{0i} and t_{0i} are the velocity and time values in the beginning *ith* region, respectively and v_i is the adsorption velocity in the *ith* region at time t. By integration form equation (13) and applying boundary condition $q_t = q_{ti}$ at $t = t_{0i}$, we have

$$q_t = \frac{1}{2}a_i t^2 + (v_{0i} - a_i t_{0i})t + q_{0i} - \frac{1}{2}a_i t_{0i}^2 \\ - (v_{0i} - a_i t_{0i})t_{0i} \tag{14}$$

where q_{0i} is the q_t value in the beginning *ith* region. q_{02} and t_{02} are the coordinates of *ssr* point. Equation (14) is named "*Kinetics of Adsorption Study in the Regions with Constant Adsorption Acceleration*" or abbreviated as KASRA equation. This equation can be abbreviated as

$$q_t = At^2 + Bt + C \tag{15}$$

where $A = \frac{1}{2}a_i$, $B = v_{0i} - a_i t_{0i}$ and $C = q_{0i} - \frac{1}{2}a_i t_{0i}^2$

$- (v_{0i} - a_i t_{0i})t_{0i}$. The KASRA equation and KASRA model were introduced by one of the authors, Babak Samiey. Finally, plateau (third) region begins at the equilibrium time, t_e and equilibrium adsorption capacity, q_e which are coordinates of *kat* point. In this region, $v_{03} = a_3 = 0$, $q_{03} = q_e$ and $t_{03} = t_e$ and equation (14) reduces to $q_t = q_e$.

Also in this study, data were analyzed by a number of equations. The pseudo-first-order equation[47] is written as follows

$$\ln(q_{e,1} - q_t) = \ln q_{e,1} - k_1 t \tag{16}$$

where k_1 is the pseudo-first-order rate constant (min^{-1}) that relates to the amount of adsorbed FA and $q_{e,1}$ denotes the calculated equilibrium adsorption capacity.

The pseudo-second-order equation[48] based on adsorption equilibrium capacity may is expressed in the form

$$\frac{t}{q_t} = \frac{1}{k_2 q_{e,2}^2} + \frac{t}{q_{e,2}} \tag{17}$$

where k_2 is the pseudo-second-order rate constant $(\text{g mg}^{-1} \text{min}^{-1})$ that relates to the amount of FA adsorbed by the solid phase and $q_{e,2}$ denotes the calculated equilibrium adsorption capacity. The rate constants obtained from the pseudo-first-order and pseudo-second-order equations change with increase in temperature in a disorder manner.[49,50] It was tried to derive pseudo-first-order equation[51] and was concluded that pseudo-first-order rate constant, k_1, increases with increase in initial adsorbate concentration, c_0. But, opposite to this conclusion, experimental results[52–55] show that k_1 values vary irregularly with increase in c_0. These two models were compared quantitatively by Δq_t, normalized standard deviations, in relation to the experimental and calculated values of q_t,

$$\Delta q_t = 100 \times \sqrt{\frac{\sum[(q_{t,\exp} - q_{t,cal})/q_{t,\exp}]^2}{(n-1)}} \tag{18}$$

where $q_{t,\exp}$ and $q_{t,cal}$ are experimental and calculated values of q_t, respectively.

The Elovich equation[56] is expressed as

$$q_t = \frac{1}{\beta}\ln(\alpha\beta) + \frac{1}{\beta}\ln t \tag{19}$$

where α is the initial adsorption rate $(\text{mg g}^{-1} \text{min}^{-1})$. β is the adsorption constant (g mg^{-1}) related to the surface coverage and is the required mass of adsorbent for adsorption of 1 mg of adsobate. The Avrami equation[57] is written as:

$$q_t = q_e\left(1 - \exp\left(-\left(k_{AV}t\right)^{n_{AV}}\right)\right) \tag{20}$$

where k_{AV} is the Avrami rate constant, and n_{AV} the Avrami exponent.

The pore-diffusion equation[58] is given as:

$$q_t = k_{dif}t^{0.5} + I \tag{21}$$

where I is proportional to the boundary layer thickness and k_{dif} is the rate constant for intraparticle diffusion.

3. 3. Effects of Temperature and FA Concentration

The effect of contact time, sizes of NiO particles and initial FA concentration on the adsorption of FA onto NiO

nanoparticles (formed at 400 °C), at 308, 318 and 328 K were studied in the FA concentration range of 6.9×10^{-5} -1.9×10^{-4} M, Figures 7(a)-7(c).

Adsorption experimental data of FA onto NiO was investigated using pseudo-first-order and pseudo-second-order kinetic equations. Data were fitted in the pseudo-second-order better than the pseudo-first-order equation, Table 4. As seen in Table 4, in each certain concentration, k_1 and k_2 values increase with increase in temperature, but in each temperature their values change irregularly with increase in FA concentration and similarly $q_{e,1}$ and $q_{e,2}$ vary irregularly with increase in temperature of FA concentration. It can be explained with respect to the used initial FA concentrations are in the second region (0.069 and 0.184 mM) and third region (0.298 mM FA) of the related adsorption isotherms (from footnotes of Tables 1 and 3) and we know that the process is exothermic in the first and second regions and endothermic in the third region. On the other hand, increase in temperature enhances the rate of transferring FA to surface of adsorbent. Competition of these two effects in 0.069 and 0.184 mM FA and their cooperation in 0.298 mM FA results in the observed trend of changes of k_1, k_2, $q_{e,1}$ and $q_{e,2}$ values.

As given in Table 4, in each certain concentration α values, from Eq. (19), increase with increase in temperature and in each temperature their values increase or keep constant with increase in FA concentration.

As seen in Table 5, the Avrami parameters, k_{AV} and n_{AV} values, change irregularly with increase in both temperature and FA concentration.

Adsorption kinetics may be controlled by film diffusion and intraparticle diffusion steps.[59] It is expected that film diffusion (external mass transfer resistance) in the aqueous phase is negligible, which is reasonable in well-shaken adsorption systems. As given in Table 5, the intercepts of adsorption kinetics profiles of q_t versus $t^{0.5}$ from
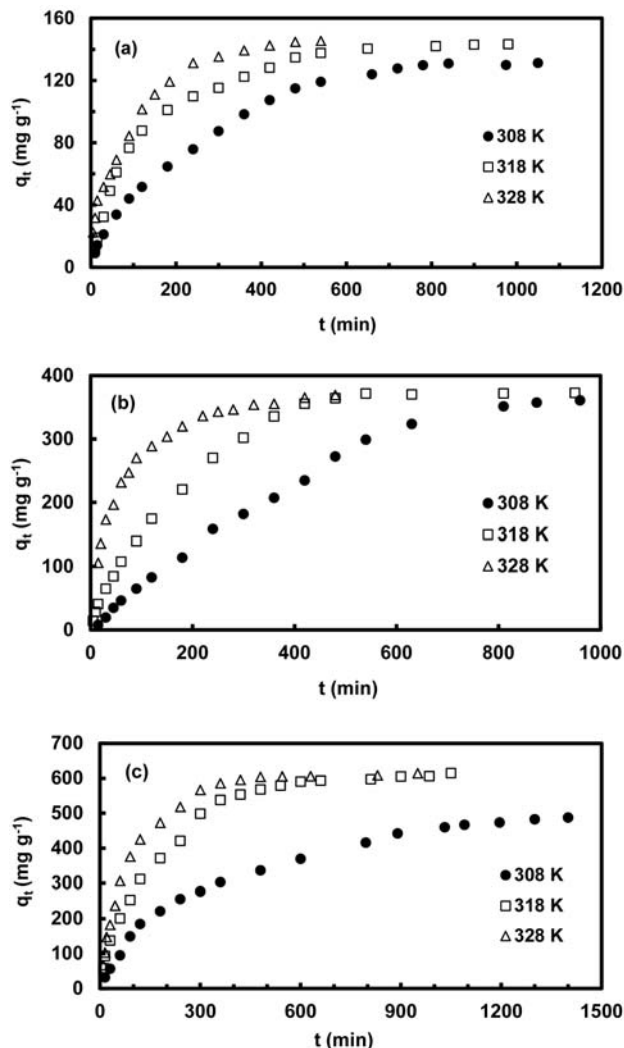

Figure 7: q_t versus t for adsorption of (a) 0.069, (b) 0.184 and (c) 0.298 mM FA on NiO nanoparticles (formed at 400 °C) at different temperatures.

Table 4. Experimental q_e values and coefficients of the pseudo-first-order, pseudo-second-order and Elovich equations for kinetics of FA adsorption on NiO nanoparticles (formed at 400 °C) from solutions at 308–328 K.

[FA] (mM)	q_e (mg g^{-1})	Pseudo-first-order			Pseudo-second-order			Elovich		
		$q_{e,1}$	$k_1 \times 10^3$	Δq_t	$q_{e,2}$	$k_2 \times 10^5$	Δq	α	β	R^2
					T=308 K					
0.069	127.67	130.96	4.04	20.8	158.98	2.93	11.91	2.495	0.066	0.973
0.184	360.90	644.16	1.12	4.99	1050.42	0.07	4.99	2.427	0.028	0.951
0.298	482.37	456.28	3.37	13.27	578.00	0.59	5.81	6.144	0.013	0.947
					T=318 K					
0.069	140.43	130.28	9.34	6.19	164.02	5.42	3.93	3.773	0.380	0.959
0.184	371.72	401.72	4.86	15.87	510.99	0.96	8.92	8.657	0.031	0.977
0.298	587.63	592.78	6.14	19.25	726.22	0.97	10.95	16.193	0.012	0.987
					T=328 K					
0.069	139.30	116.10	18.2	26.22	139.86	16.1	17.80	11.611	0.055	0.985
0.184	354.12	343.87	19.1	2.26	400.80	5.73	2.85	19.921	0.011	0.994
0.298	585.58	550.20	12.9	1.84	724.64	1.56	5.15	19.758	0.009	0.993

Dimension of $q_{e,1}$ and $q_{e,2}$ is in mg·g^{-1}. Dimensions of k_1 and k_2 are in min^{-1} and g mg^{-1} min^{-1}, respectively. Dimensions of α and β are in mg g^{-1} min^{-1} and g mg^{-1}, respectively.

Table 5. Coefficients of the Avrami equation and pore-diffusion equation (the first and second regions) for kinetics of FA adsorption on NiO nanoparticles (formed at 400 °C) at 308–328 K.

[FA] (mM)	Avrami			Pore-diffusion (1st)			Pore-diffusion (2nd)		
	k_{AV}	n_{AV}	R^2	k_{dif}	I	R^2	k_{dif}	I	R^2
T = 308 K									
0.069	4.12×10^{-3}	0.838	0.989	5.54	–8.73	0.997	5.72	–11.51	0.996
0.184	2.86×10^{-3}	1.127	0.989	10.34	–33.36	0.993	18.16	–130.05	0.994
0.298	2.94×10^{-3}	0.856	0.992	20.39	–49.41	0.991	12.31	66.49	0.997
T = 318 K									
0.069	6.90×10^{-3}	0.840	0.991	10.54	–22.05	0.990	4.31	40.15	0.987
0.184	6.11×10^{-3}	0.954	0.986	15.66	–20.59	0.999	19.77	–41.96	0.995
0.298	5.95×10^{-3}	0.819	0.990	29.75	–28.59	0.995	28.90	–12.46	0.988
T = 328 K									
0.069	1.03×10^{-2}	0.624	0.979	8.18	6.55	0.953	8.82	1.74	0.998
0.184	1.57×10^{-2}	0.715	0.994	27.58	11.92	0.990	1.51	163.63	0.992
0.298	9.62×10^{-3}	0.862	0.992	52.11	–101.12	0.992	23.36	159.97	0.993

Dimensions of k_{dif}, I and k_{AV} are in mg g^{-1} min$^{-0.5}$, mg g^{-1} and min$^{-0.5}$, respectively. n_{AV} is dimensionless. Boundaries of the first and second regions are around t_{02} and q_{02} values, given in Table 7.

Table 6. Coefficients of the KASRA equation for kinetics of FA adsorption on NiO nanoparticles (formed at 400 °C) at 308–328 K.

[FA] (mM)	First region				Second region			
	A	B	C	R^2	A	B	C	R^2
T = 308 K								
0.069	-2.44×10^{-3}	0.706	1.267	0.993	-1.97×10^{-4}	0.293	18.351	0.998
0.184	-9.95×10^{-4}	0.800	1.034	0.996	-4.01×10^{-4}	0.771	-9.325	0.996
0.298	-2.69×10^{-3}	1.880	-1.740	0.996	-1.88×10^{-4}	0.507	137.861	0.998
T = 318 K								
0.069	-4.37×10^{-3}	1.246	-0.886	0.999	-1.56×10^{-4}	0.217	65.233	0.996
0.184	-1.30×10^{-2}	2.493	2.170	0.995	-1.14×10^{-3}	1.237	39.190	0.999
0.298	-4.80×10^{-2}	6.180	1.494	0.995	-1.71×10^{-3}	1.794	105.568	0.996
T = 328 K								
0.069	-1.70×10^{-2}	2.146	0.357	0.995	-9.82×10^{-4}	0.635	36.204	0.993
0.184	-6.30×10^{-2}	7.417	4.995	0.988	-1.88×10^{-3}	1.154	173.973	0.992
0.298	-3.65×10^{-2}	7.132	3.090	0.992	-2.38×10^{-3}	1.873	217.290	0.988

Dimensions of A, B and C are in mg g^{-1} min^{-2}, mg g^{-1} min^{-1} and mg g^{-1}, respectively.

Table 7. Experimental t_e, q_e, t_{02} and q_{02} values and coefficients of the KASRA equation for kinetics of FA adsorption on NiO nanoparticles (formed at 400 °C) at 308–328 K.

[FA] (mM)	t_e (min)	q_e (mg g^{-1})	t_{02} (min)	q_{02} (mg g^{-1})	First region		Second region	
					a_1	v_{01}	a_2	v_{02}
T = 308 K								
0.069	720	127.67	120	51.60	-4.88×10^{-3}	0.706	-3.94×10^{-4}	0.246
0.184	960	360.90	120	82.70	-1.99×10^{-3}	0.800	-8.02×10^{-4}	0.675
0.298	1300	482.37	120	184.47	-5.38×10^{-3}	1.880	-3.76×10^{-4}	0.462
T = 318 K								
0.069	650	140.43	120	87.77	-8.74×10^{-3}	1.246	-3.12×10^{-4}	0.180
0.184	540	371.72	60	107.58	-2.60×10^{-2}	2.493	-2.28×10^{-3}	1.100
0.298	540	587.63	60	200.46	-9.60×10^{-2}	6.180	-3.42×10^{-3}	1.589
T = 328 K								
0.069	360	139.30	60	69.04	-3.40×10^{-2}	2.146	-1.96×10^{-3}	0.517
0.184	360	354.12	60	231.70	$-0,126$	7.417	-3.76×10^{-3}	0.928
0.298	360	585.68	60	306.17	-7.30×10^{-2}	7.132	-4.76×10^{-3}	1.587

Dimensions of a_1 and a_2 are in mg g^{-1} min^{-2} and those of v_{01} and v_{02} are in mg g^{-1} min^{-1}. In the first region, t_{01} and q_{01} values are equal to zero. q_e values in each FA concentration and each temperature were shown in Table 4.

Eq. (21), for the initial steeper and second regions have negative values which suggests that the boundary-layer effect is close to minimum and diffusion of the FA molecules into the NiO nanoparticles (intraparticle diffusion) is the main rate-controlling step.[59,60]

Kinetics of FA adsorption on NiO nanoparticles at 308–328 K was studied by the KASRA equation which shows that there are two regions before plateau, Tables 6 and 7.

Results obtained from Table 7 are as follows:

1 – In each kinetic experiment, with increase in time, the number of surface adsorption sites and FA concentration decrease and thus the sign of adsorption acceleration, a_i, is negative and adsorption velocity, v_i, value decreases.

2 – In each certain temperature and FA concentration, v_{0i} values decrease and a_{0i} values become less negative from the first region to the second one. This is due to decrease in FA concentration and decrease in the number of unoccupied sites on the surface of NiO nanoparticles.

3 – Similar to α values obtained from the Elovich equation (Table 4), initial velocity values in the first region (v_{01}), increase with increase in temperature in each

certain FA concentration or with increase in FA concentration in each temperature. This is due to similar increase in k_{dif} values (Table 4) under above-mentioned conditions in the first region.

4 – In each region, with increase in temperature in each certain FA concentration, q_{02} values increase and a_{01} and a_{02} values become more negative.

3. 4. Effects of Size of Nanoparticles and Shaking Rate

Adsorption of FA on different sizes of NiO nanoparticles (formed at 250, 400 and 600 °C) in 0.184 mM FA was studied at 318 K and 80 rpm, Figure 8 and Tables 8 and 9. XRD spectra of these samples, Figure 2, showed that with increase in the temperature of NiO nanoparticles formation from 250 to 400 to 600 °C, their sizes change from 25.1 to 13.1 to 30.3 nm, respectively. As shown in Table 9, with increase in size of NiO nanoparticles from the sample formed in 400 °C compared to the sample formed at 600 °C, adsorption acceleration values of the first and second regions of them become less negative, their

Table 8. Coefficients of the KASRA equation for kinetics of adsorption of FA from 0.184 mM FA solution on NiO nanoparticles (formed at different temperatures) at 318 K and various shaking rate.

NiO formed at	First region				Second region			
	A	*B*	*C*	R^2	*A*	*B*	*C*	R^2
At 40 rpm								
400 °C	-1.10×10^{-2}	1.917	-1.013	0.996	-6.37×10^{-4}	0.991	-8.507	0.994
At 80 rpm								
250 °C	-1.39×10^{-2}	4.058	-1.971	0.994	-6.51×10^{-4}	0.740	197.930	0.992
400 °C	-1.30×10^{-2}	2.493	2.170	0.995	-1.14×10^{-3}	1.237	39.190	0.999
600 °C	-1.41×10^{-3}	0.693	0.301	0.999	-1.72×10^{-4}	0.332	24.296	0.998
At 120 rpm								
400 °C	-3.10×10^{-2}	3.263	0.439	0.999	-2.87×10^{-3}	2.002	6.252	0.995

Dimensions of *A*, *B* and *C* are in mg g^{-1} min^{-2}, mg g^{-1} min^{-1} and mg g^{-1}, respectively.

Table 9. Experimental t_e, q_e, t_{02} and q_{02} values and coefficients of the KASRA equation for kinetics of adsorption of FA from 0.184 mM FA solution on NiO nanoparticles (formed at different temperatures) at 318 K and various shaking rate.

NiO formed at	t_e (min)	q_e (mg g^{-1})	t_{02} (min)	q_{02} (mg g^{-1})	First region		Second region	
					a_1	v_{01}	a_2	v_{02}
At 40 rpm								
400 °C	840	372.85	90	82.70	-2.20×10^{-2}	1.917	-1.27×10^{-3}	0.776
At 80 rpm								
250 °C	652	406.29	90	250.43	-2.78×10^{-2}	4.058	-1.79×10^{-3}	0.579
400 °C	540	371.72	60	107.58	-2.60×10^{-2}	2.493	-2.28×10^{-3}	1.100
600 °C	871	182.76	120	63.16	-2.82×10^{-3}	0.693	-3.44×10^{-4}	0.291
At 120 rpm								
400 °C	360	360.74	45	84.48	-6.20×10^{-2}	3.263	-5.74×10^{-3}	1.744

Dimensions of a_1 and a_2 are in mg g^{-1} min^{-2} and those of v_{01} and v_{02} are in mg g^{-1} min^{-1}. In the first region, t_{01} and q_{01} are equal to zero.
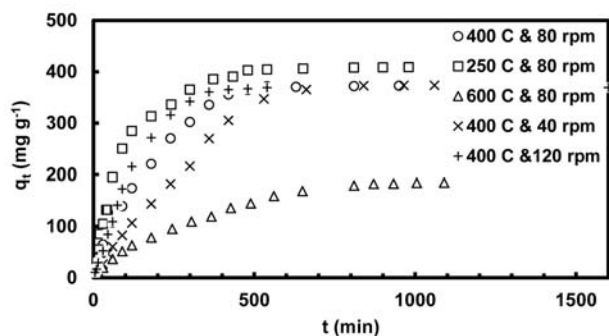
Figure 8: q_t versus t for adsorption of 1.84 mM FA on NiO nanoparticles (formed at different temperatures) at various shaking rates.

q_{02}, q_e, v_{01} and v_{02} values decrease and t_e values of them increase. On the other hand, q_{02} and q_e values of the nanostructure formed in 250 °C (in spite of its larger size) are higher than those of the sample formed in 400 °C. It seems that this observation is due to the structural change in the sample formed in 250 °C that is because of the presence of metallic nickel in its structure. Also, in a series of experiments, shaking rate of 0.184 mM FA samples at 318 K was increased from 40 to 120 rpm. As shown in Figure 8 and Table 9, in these processes, adsorption acceleration in both regions is negative in sign and initial adsorption velocity of the first and second regions increases with increasing shaking rate. Also, as observed in Table 9, with increase in shaking rate of these samples their t_e and q_{02} values decrease and increase, respectively.

4. Conclusions

NiO nanoparticle, prepared by thermal decomposition of the tris(ethylenediamine) Ni(II) nitrate complex, was used as adsorbent to remove negatively charged fuchsine acid (FA) from aqueous solution. In the used concentration range of FA, its adsorption isotherms on NiO nanoparticles (formed at 400 °C) according to ARIAN model were three-region. Adsorption process in the first, second and third regions was studied by the Henry's law, Temkin and Langmuir-like equations, respectively and analysis of data showed that the process is exothermic in the first and second regions and endothermic in the third region. IR spectra showed that FA interacts with -OH groups of NiO nanoparticles. With decrease in pH values more amount of NiO nanoparticles dissolve and q_e values decrease. Data of adsorption kinetics were analyzed by the pseudo-first-order, pseudo-second-order, Elovich, Avrami, pore-diffusion and KASRA equations. The KASRA equation showed that at 40, 80 and 120 rpm and different temperatures, the sign of adsorption acceleration in the first and second regions of adsorption kinetics of FA on NiO nanopparticles was negative and with increase in FA concentration or temperature or shaking rate, initial adsorption velocity values of each region increase.

5. References

1. S. Tsuda, M. Murakami, N. Matsusaka, K. Kano, K. Taniguchi, Y. F. Sasaki, *Toxicol. Sci.* **2001**, *61*, 92–99.
2. B. Przybojewska, B. Baranski, E. Spiechowiecz, K. Sitarrek, *Toxicol. Lett.* **1998**, *40*, 183–192.
3. J. Pan, B. Guan, *J. Hazard. Mater.* **2010**, *183*, 341–346.
4. X. Tan, N. N. Kyaw, W. K. Teo, K. Li, *Sep. Purif. Technol.* **2006**, *52*, 110–116.
5. A. Latifoglu, M. D. Gurol, *Water Res.* **2003**, *37*, 1879–1889.
6. F. J. Beltrán, J. M. Encinar, M. A. Alonso, *Ind. Eng. Chem. Res.* **1998**, *37*, 32–40.
7. I. K. Konstantinou, T. A. Albanis, *Applied Catalysis B: Environmental* **2004**, *49*, 1–14.
8. K. Ravikumar, S. Krishnan, S. Ramalingam, K. Balu, *Dyes and Pigments* **2007**, *72*, 66–74.
9. W. Liu, Y. Chao, X. Yang, H. Bao, S. Qian, *J. Ind. Microbiol. Biotechnol.* **2004**, *31*, 127–132.
10. J. M. Bastidas, P. Pinilla, E. Cano, J. L.Polo, S. Miguel, *Corros. Sci.* **2003**, *45*, 427–449.
11. http://en.wikipedia.org/wiki/Fuchsine
12. M. Z. bin Hussein, A. Hj Yahaya, M. Shamsul, H. M. Salleh, T. Yap, J. Kiu, *Mater. Lett.* **2004**, *58*, 329–332.
13. T. , Y., *Chem. Eng. J.*, 123–131.
14. B. Xu, B. *J. Chin. Chem. Soc.* **2010**, *57*, 309–315.
15. S. Michael Anto, G. Annadurai, *Research Journal of Nanoscience and Nanotechnology* **2012**, *2*, 31–45.
16. C. L. Chen, X. K. Wang, M. Nagatsu, *Environ. Sci. Technol.* **2009**, *43*, 2362–2367.
17. A. Afkhami, R. Moosavi, *J. Hazard. Mater.* **2010**, *174*, 398–403.
18. T. G. Venkatesha, R. Viswanatha, Y. Arthoba Nayaka, B. K. Chethana, *Chem. Eng. J.* **2012**, *198–199*, 1–10.
19. V. Belessi, G. Romanos, N. Boukos, D. Lambropoulou, C. Trapalis, *J. Hazard. Mater.* **2009**, *170*, 836–844.
20. P. Liu, L. Zhang, *Sep. Purif. Technol.* **2007**, *58*, 32–39.
21. F. M. Machado, C. P. Bergmann, T. H. M. Fernandes, E. C. Lima, B. Royer, T. Calvete, S. B. Fagan, *J. Hazard. Mater.* **2011,** *192,* 1122–113.
22. E. D. Vega, G. E. Narda, F. H. Ferretti, *J. Colloid Interface Sci.* **2003,** *268,* 37–42.
23. M. Singh, D. Nguyen, T. Ulbrich, N. Strnadová, F. Stepánek, *J. Solid State Chem.* **2010**, *183*, 2979–2986.
24. V. Srivastava, C. H. Weng, V. K. Singh, Y. C. Sharma, *Chem. Eng. Data* **2011**, *56*, 1414–1422.
25. Y. Zhuang, Y. Yang, G. Xiang, X. Wang, *J. Phys. Chem. C* **2009**, *113*, 10441–10445.
26. W. Wei, X. Jiang, L. Lu, X. Yang, X. Wang, *J. Hazard. Mater.* **2009**, *168*, 838–842.
27. F. Li, H. Y. Chen, C. M. Wang, K. A. Hu, *J. Electroanal. Chem.* **2002**, *531*, 53–60.
28. I. Hotovy, J. Huran, L. Spiess, S. Hascik, V. Rehacek, *Sens. Actuators B: Chem.* **1999**, *57*, 147–152.
29. F. B. Zhang, Y. K. Zhou, H. L. Li, *Mater. Chem. Phys.* **2004**, *83*, 260–264.
30. M. Ghosh, K. Biswas, A. Sundaresan, C. N. R. Rao, *J. Mater.*

Chem. **2006**, *16*, 106–111.

31. C. G. Granqvist (Ed.): Handbook of Inorganic Electrochromic Materials, Elsevier; Amsterdam, **1995**.

32. S. Farhadi, Z. Roostaei-Zaniyani, *Polyhedron* **2011**, *30*, 971–975.

33. H. P. Klug, L. E. Alexander: X-ray Diffraction Procedures, 2nd Ed., Wiley, New York, **1964**.

34. M. Huang, C. Xu, Z. Wu, Y. Huang, J. Lin, J. Wu, *Dyes Pigments*, **2008**, *276*, 327–334.

35. B. Samiey, S. Golestan, *Cent. Eur. J. Chem.* **2010**, *8*, 361–369.

36. I. Langmuir, *J. Am. Chem. Soc.* **1918**, *40*, 1361–1403.

37. M. Boudart, G. Djega-Mariadassou: Kinetics of Heterogeneous Catalytic Reactions, Princeton University Press, **1984**, p 132.

38. M. M. Dubinin, *Carbon* **1985**, *23*, 373–380.

39. J. P. Hobson, *J. Phys. Chem.* **1969**, *73*, 2720–2727.

40. J. A. Lewis, *J. Am. Ceram. Soc.* **2000**, *83*, 2341–2359.

41. S. Paria, C. Manohar, K. C. Khilar, *Ind. Eng. Chem. Res.* **2005**, *44*, 3091–3098.

42. J. D. Fisk, M. Rooth, A. M. Shaw, *J. Phys. Chem. C* **2007**, *111*, 2588–2594.

43. F. Tiberg, B. Jönsson, B. Lindman, *Langmuir* **1994**, *10*, 3714–3722.

44. P. Supaphol, J. E. Spruiell, *J. Macromol. Sci. Phys. B* **2000**, *39*, 257–277.

45. P. Supaphol, *Thermochim. Acta* **2001**, *370*, 37–48.

46. C. Albano, R. Sciamanna, R. Gonzalez, J. Papa, O. Navarro, *Eur. Polym. J.* **2001**, *37*, 851–860.

47. S. Lagergern, Handlinger **1898**, *24*, 1–39.

48. Y. S. Ho, G. Mckay, *Water Res.* **2000**, *34*, 735–742.

49. J. M. Borah, S. Mahiuddin, *J. Colloid Interface Sci.* **2008**, *322*, 6–12.

50. S. Karaca, A. Gürses, M. Ejder, M. Açýkyýldýz, *J. Colloid Interface Sci.* **2004**, *277*, 257–263.

51. S. Azizian, *J. Colloid Interface Sci.* **2004**, *276*, 47–52.

52. B. H. Hameed, M. I. El-Khaiary, *J. Hazard. Mater.* **2008**, *159*, 574–579.

53. P. Shuchuan, W. Shisheng, C. Tianhu, J. Shaotong, H. Chuanhu, *Acta Geologica Sinica* **2006**, *80*, 236–242.

54. C. F. Chang, C. Y. Chang, K. H. Chen, W. T. Tsai, J. L. Shie, Y. H. Chen, *J. Colloid Interface Sci.* **2004**, *277*, 29–34.

55. X. Yang, B. Al-Duri, *J. Colloid Interface Sci.* **2005**, *287*, 25–34.

56. C. W. Cheung, J. F. Porter, G. McKay, *J. Chem. Technol. Biotechnol.* **2000**, *75*, 963–970.

57. M. Avrami, *J. Chem. Phys.* **1939**, *7*, 1103–1112.

58. G. McKay, V. P. Poots, *J. Chem. Technol. Biotechnol.* **1980**, *30*, 279–292.

59. A. R. Cestari, E. F. S. Vieira, A. A. Pinto, E. C. N. Lopes, *J. Colloid Interface Sci.* **2005**, *292*, 363–372.

60. B. Samiey, M. Rafi Dargahi, *Cent. Eur. J. Chem.* **2010**, *8*, 906–912.

Povzetek

Proučevali smo adsorpcijo fuksin žveplove kisline (FA) iz vodne raztopine na delcih NiO, ki smo jih pripravili s termično dekompozicijo iz tris(etilendiamin)Ni(II) nitratnega kompleksa. Izkazalo se je, da proces adsorpcije lahko razdelimo v tri področja. V prvih dveh je proces eksotermen, v tretjem pa endotermen. Kinetiko adsorpcije smo raziskovali z nekaterimi modeli, kot so KASRA, psevdo prvi red, psevdo drugi red, Elovich, Avrami in enačba za difuzijo v porah. Z uporabo KASRA enačbe smo ugotovili, da se z naraščanjem koncentracije FA v raztopini, temperature ali hitrosti mešanja začetna hitrost adsorpcije poveča.